AGU PUBLICATIONS

JGR

Journal of Geophysical Research: Planets

RESEARCH ARTICLE

10.1002/2014JE004700

Key Points:
- The effect of the sources located along the Tiger Stripes on the exosphere
- Methodology of the updated multiplume model is presented
- The model results are constrained by Cassini's INMS and UVIS measurements

Correspondence to:
V. Tenishev,
vtenishe@umich.edu

Citation:
Tenishev, V., D. C. S. Öztürk, M. R. Combi, M. Rubin, J. H. Waite, and M. Perry (2014), Effect of the Tiger Stripes on the water vapor distribution in Enceladus' exosphere, *J. Geophys. Res. Planets*, *119*, 2658–2667, doi:10.1002/2014JE004700.

Received 23 JUL 2014
Accepted 30 OCT 2014
Accepted article online 17 NOV 2014
Published online 23 DEC 2014

Effect of the Tiger Stripes on the water vapor distribution in Enceladus' exosphere

Valeriy Tenishev[1], Doğa Can Su Öztürk[1], Michael R. Combi[1], Martin Rubin[2], Jack Hunter Waite[3], and Mark Perry[4]

[1]Department of Atmospheric, Oceanic and Space Sciences, University of Michigan, Ann Arbor, Michigan, USA, [2]Physikalisches Institut, University of Bern, Bern, Switzerland, [3]Southwest Research Institute, San Antonio, Texas, USA, [4]Applied Physics Laboratory, Johns Hopkins University, Laurel, Maryland, USA

Abstract The jet activity emanating from Enceladus' exosphere south pole region observed by Cassini is a subject of intensive study. The in situ and remote sensing observations performed since 2005 triggered an active modeling campaign. Such modeling is essential for better understanding of the measurements performed by individual instruments as well as to link them for a more complete picture of the volatile and ice grain distribution in Enceladus' exosphere. This paper is focused on the investigation of the effect that diffuse gas sources along the Tiger Stripes have on distribution of the water vapor in Enceladus' exosphere using the updated version of our multiplume model. We have found that accounting for the gas production by Tiger Stripes is critical for interpretation of the Cassini data. According to our calculations, sources along the Tiger Stripes (apart from those originally identified by Spitale and Porco (2007)) must contribute about 23–32% to the total plume source rate, which varies in the range of (6.4–29) $\times 10^{27}$ s^{-1}. The effect of the previously unidentified source suggested in the paper is found to be critical for explaining the Ultraviolet Imaging Spectrograph 2007 and 2010 observations in the whole range of the elapsed times.

1. Introduction

The gas and ice grain plumes discovered by Cassini in 2005 made Enceladus an object of increased scientific interest. The observed activity in the south pole region raised questions regarding the source of the plumes' material, mechanisms of its delivery to the surface, and distribution of the dust and ice grains [*Hedman et al.*, 2009; *Postberg et al.*, 2011; *Ingersoll and Ewald*, 2011] and gas [*Spencer and Nimmo*, 2013] in the exosphere.

In this work we investigate the potential effect of diffuse or multiple small gas sources along the Tiger Stripes on the water vapor distribution in Enceladus' exosphere [*Hansen et al.*, 2011]. Even though most of plume's gas and ice grain material is ejected by the vents [*Spitale and Porco*, 2007], the gas production by the fissures is essential for understanding Cassini observations.

The effect of the Tiger Stripes on water vapor distribution in the exosphere has been studied with the updated version of our multiplume model [*Tenishev et al.*, 2010] that now includes the gas production from the vents, the fissures, and a global spherical source. The paper describes the methodology of the model, and presents comparisons of the model results with Cassini Ultraviolet Imaging Spectrograph (UVIS), and Ion and Neutral Mass Spectrometer (INMS) observations, and assesses the relative source rates of the individual gas vents [*Spitale and Porco*, 2007] as well as the diffuse sources along the Tiger Stripes.

2. Modeling of Enceladus' Neutral Gas Plume

Collisionless regime in Enceladus' exosphere does not allow one to use fluid methods for modeling of the gas distribution. For this reason all models used to analyze the plume observations treat the gas distribution based on a kinetic approach. Three classes of models were used in the previous analyses: (1) numerical Monte Carlo, where model particles are produced at the locations of the observed vents [*Smith et al.*, 2010; *Burger et al.*, 2007; *Waite et al.*, 2006; *Tian et al.*, 2007; *Tenishev et al.*, 2010]; 2) analytical, where a Maxwellian distribution of the gas is assumed at the vent locations and density is calculated using Liouville's theorem [*Tenishev et al.*, 2010; *Dong et al.*, 2011]; and 3) analytical, where the column density is directly calculated using occultation measurements [*Hansen et al.*, 2006, 2008, 2011]. The summary of the results obtained with these models is presented in Table 1.

Table 1. Summary of Enceladus' Exosphere Modeling Results

Observation	Total Production Rate (s^{-1})	Model Type	Reference
INMS E2, E3, E5	10^{27}–10^{28}	Monte Carlo	*Smith et al.* [2010]
INMS E2; UVIS 2005	10^{28}	Monte Carlo	*Burger et al.* [2007]
INMS E3, E5, E7	$(1.5–3.5)\times10^{28}$	Analytic	*Dong et al.* [2011]
INMS E2	$(1.5–4.5)\times10^{26}$	Monte Carlo	*Waite et al.* [2006]
UVIS 2005	$(5–10)\times10^{27}$	Analytic	*Hansen et al.* [2006]
UVIS 2005	$(4–6)\times10^{27}$	Monte Carlo	*Tian et al.* [2007]
UVIS 2007	6.5×10^{27}	Analytic	*Hansen et al.* [2008]
INMS E3, E5; UVIS 2005	2.6×10^{28}	Analytic, Monte Carlo	*Tenishev et al.* [2010]
UVIS 2005, 2007, 2010	$(5.8–7.4)\times10^{27}$	Analytic	*Hansen et al.* [2011]

3. Multiplume Model

The amount of the available data does not allow the derivation of the exact condition of the gas sources at the surface. This makes forward modeling highly problematic. Instead, we use a phenomenological model where a gas density is determined by summing contributions of a uniform spherically symmetric source, eight vents identified by *Spitale and Porco* [2007], and fissures located along the Tiger Stripes. The number density that is due to the latter two is calculated by integrating the appropriate gas velocity distribution function defined at the surface. We assume that at the surface the gas is in a state of the thermodynamics equilibrium and can be described by the convected Maxwellian velocity distribution function. The parameters of the distribution function as well as the source rates are determined by fitting the model number and column densities to the observations.

The primary difference between our model and that by *Dong et al.* [2011] who have used a similar approach for evaluation of the exospheric densities is in calculation of the distribution function moments. *Dong et al.* [2011] approximate the distribution function moment integrals in order to evaluate them analytically, while in our model all integrals are evaluated numerically.

3.1. Gas Vents

Gas ejected into Enceladus' exosphere may be in a collision-dominated regime only close to the surface. Neglecting the limited region where collision coupling could be important as well as ionization and dissociations reactions (rates of the loss processes are in, e.g., *Burger et al.* [2007]), we calculate a number density in the exosphere that is due to a point source with Liouville's theorem.

Particles are ejected into the plume with speed (about 1 km/s) that significantly exceeds the escape speed of Enceladus (235 m/s). As a result, gravity does not significantly affect their trajectories in the region where Cassini observations were performed as was shown in our earlier work [*Tenishev et al.*, 2010]. This allows us to consider the individual sources as axially symmetric, which significantly simplifies the mathematical description of the gas flow and reduces the number of free model parameters. As a result, number density of water vapor in the exosphere that is due to an individual gas vent can be evaluated as

$$n(\mathbf{x}) = \begin{cases} \frac{A_p}{r^2}\int v^2 \exp\left(-\beta^2\left[v^2\sin^2\theta + (v\cos\theta - v_p)^2\right]\right)\mathrm{d}v & \text{if} \quad ((\mathbf{x}-\mathbf{r}_p)\cdot\mathbf{r}_p) \geq 0 \\ 0 & \text{otherwise,} \end{cases} \tag{1}$$

where $\mathbf{x}$ is a point where a number density is calculated, (r, ϕ, θ) are coordinates of the point $\mathbf{x}$ in a spherical coordinate frame associated with the vent, $\mathbf{r}_p$ is the vent location, v_p is the bulk speed of the gas flow ejected from the vent, $\beta = \sqrt{m_{H_2O}/2\,\mathrm{kT}}$, and A_p is a normalization constant defined as

$$A_p = \frac{F_p}{\int\int\int v^3 \exp\left(-\beta^2\left[v^2\sin^2\theta + (v\cos\theta - v_p)^2\right]\right)\mathrm{d}v\mathrm{d}\theta\mathrm{d}\phi}. \tag{2}$$

Here F_p is the total source rate (s^{-1}) of the vent. The integration limits in equation (2) are constrained by the condition $\left(\mathbf{v}(v,\phi,\theta)\cdot\mathbf{r}_p\right) \geq 0$. Here $\mathbf{v}$ is the velocity vector that corresponds to that defined in the spherical frame by the combinations of (v, ϕ, θ). The integrals in equations (1) and (2) are calculated numerically. Positions of the individual vents used in the model are given in Table 2.

Table 2. Position and Direction of Enceladus' Dust Jets[a]

		Position on the Surface		Direction of the Dust Jets	
Vent	Tiger Stripe	Lat.[b]	W. Lon.[b]	Zenith Angle[c]	Azimuth Angle[d]
I	Baghdad	81.5	31.2	9.7	228.7
II	Damascus	79.2	313.2	6.8	93.8
III	Damascus	81.2	294.2	30.2	83.2
IV	Alexandria	73.2	148.4	3.7	110.0
V	Cairo	78.7	72.6	6	229.8
VI	Baghdad	87.1	237.0	10.2	187.6
VII	Baghdad	74.7	28.9	20.8	352.5
VIII	Cairo	82.1	115.5	6.8	127.7

[a]The table is taken from *Spitale and Porco* [2007].
[b]Latitudes (Lat.) are planetographic and longitudes (W. Lon.) increase toward the west.
[c]Zenith angle is measured in degrees between the vertical direction and the direction of the plume.
[d]Azimuth angle is measured in degrees clockwise from local north (that is, eastward to an observer standing on the surface facing north).

3.2. Tiger Stripes

Thermal emission observed with Composite Infrared Spectrometer (CIRS) onboard Cassini [*Spencer et al.*, 2013] and plume jets observed with UVIS [*Hansen et al.*, 2008, 2011] suggest that the gas production of the Tiger Stripes can have a significant influence on the distribution of gas in Enceladus's exosphere. The large number of the observed jets (e.g., Cassini press release image PIA 10356, http://photojournal.jpl.nasa.gov/catalog/PIA10356) makes it impossible to simulate the fissure gas production by modeling individual jets.

In order to reduce the number of the model parameters, we assume uniform gas production along the length of the fissure. CIRS observations of the thermal emission suggest possible variation of the source rate, which was accounted for in our model by introducing additional fissures located at the regions with higher temperature.

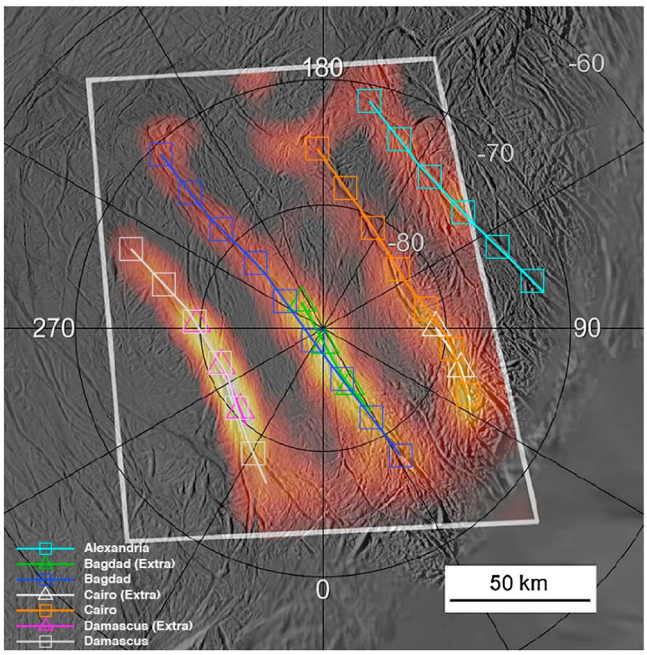

Figure 1. Location of the thermal emission observed on Enceladus' surface with Cassini CIRS on 12 March 2008 and the model of the Tiger stripes used in the simulations. (Cassini press release image PIA 10361 NASA/JPL/GSFC/SwRI/SSI. Taken from http://ciclops.org/view/4917/Jet_Spots_in_Tiger_Stripes?js=1.)

For modeling of the gas production by the Tiger Stripes, we have used two families of the fissures: "normal" (Damascus, Bagdad, Cairo, and Alexandria) and "extra" (Damascus (extra), Bagdad (extra), and Cairo (extra)). The extra fissures are located at the regions of the enhanced surface temperature observed by CIRS. Each fissure has a unique source rate that is constant along its length. Each family of the fissures has its own temperature, which also is constant along the stripes. The set of the model fissures as well as the observed thermal emission [*Howett et al.*, 2011] are presented in Figure 1.

The fissures are modeled by a set of the vertically directed point sources described by equation (1). These point sources are uniformly distributed along the stripes, which results in their uniform gas production. In the model runs presented here the sources were separated by 6.5 km, which resulted in total of 102 point sources used for simulating of the gas production from the fissures.

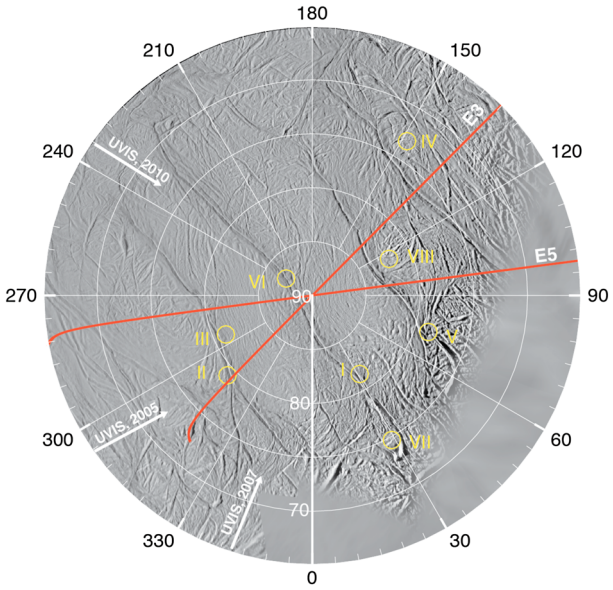

Figure 2. Ground tracks of INMS E3 and E5 flybys, pointing direction of UVIS during 2005, 2007, and 2010 observations and locations of the observed dust jets. Yellow circles are the locations of the vents [*Spitale and Porco*, 2007].

3.3. Spherically Symmetric Background Gas Distribution

The background gas distribution is assumed in the form $n = c_0 + c_1 r^{\alpha}$, where c_0 and c_1 are the model constants and r is the distance to the center of Enceladus [*Burger et al.*, 2007; *Smith et al.*, 2010; *Dong et al.*, 2011; *Waite et al.*, 2006; *Tenishev et al.*, 2010]. The constant part of the distribution is commonly attributed to Enceladus' neutral torus [*Johnson et al.*, 2006]. The power law component of the background density is attributed to molecules sputtered from Enceladus' surface [*Waite et al.*, 2006] or previously ejected from Enceladus' plumes and Tiger Stripes into the exosphere [*Smith et al.*, 2010]. The power index varies in the range from −2.3 [*Burger et al.*, 2007] up to −2 [*Dong et al.*, 2011; *Waite et al.*, 2006; *Tenishev et al.*, 2010]. In this work we have used $\alpha = -2$.

4. Results

In this work we have applied our multiplume model to analyze the INMS E3 and E5 flybys [*Teolis et al.*, 2010] and UVIS 2005, 2007, and 2010 observations [*Hansen et al.*, 2006, 2008, 2011]. Ground tracks of Cassini during INMS observations as well as the pointing directions of UVIS are presented in Figure 2.

In order to determine the effect of the Tiger Stripes on the distribution of water vapor in Enceladus' exosphere, we have compared modeled UVIS and INMS observations when the gas ejection from the fissures has been neglected (Case 1) with those when it has been taken into account (Case 2).

In order to minimize the number of the model variables, only the production rate was used to fit the observations, while other physical parameters of the fissures and jets (such as a gas temperature and bulk velocity) were fixed. The numerical values of the latter have been evaluated by fitting the model to the Case 1.

The best fit was achieved for the fissure temperature of 180 K and bulk velocities of 350 m s^{-1} and 950 m s^{-1} for the normal and extra fissures, respectively. These values are consistent with Cassini CIRS measurement of the surface temperature (at least 170 K) and the gas thermal velocity (at least 450 m s^{-1}) [*Spencer et al.*, 2009; *Hansen et al.*, 2011; *Goguen et al.*, 2013]. The best fit gas temperature and bulk velocity at the vents are given in Table 3.

The best fit parameters of the background gas distribution are $c_0 = 2.7 \times 10^{10}$ and $c_1 = 1.6 \times 10^{23}$. The number density due to the background population is at least 2 orders below the peak exospheric density measured by INMS as shown in Figure 3. According to our simulations, the column density due to the background population does not exceed 1–2% at the peak of the column density during UVIS observations.

Table 3. Bulk Velocity and Temperature at the Vents

Vent	Bulk Velocity (m/s)	Temperature (K)
I	800	190
II	1312	170
III	600	210
IV	1100	190
V	1030	190
VI	740	194
VII	1338	206
VIII	580	190

It is important to note that a production rate, bulk velocity, and temperature of a source are not completely independent. It is a combination of these parameters that defines a value of the local number density as shown in equation (1).

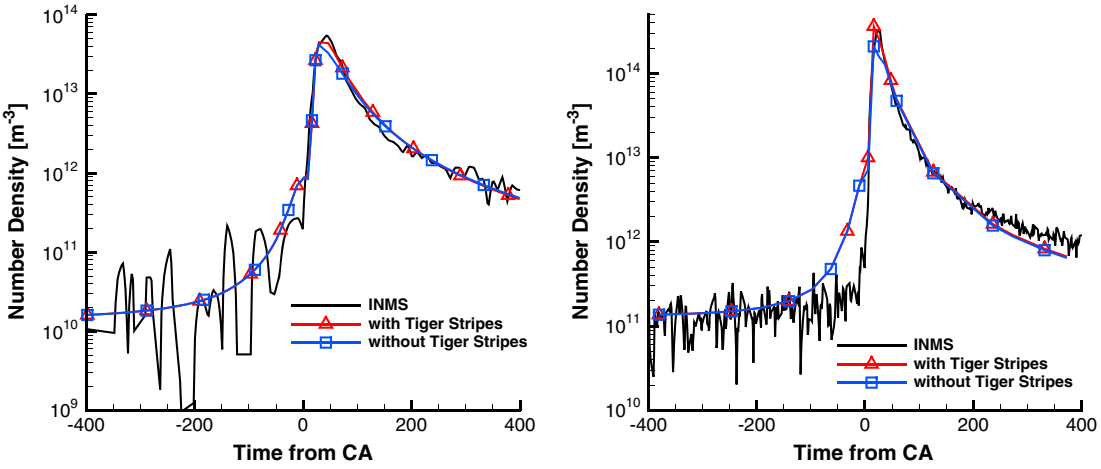

Figure 3. Comparison of the model results with the INMS observations [*Teolis et al.*, 2010] during (left) E3 and (right) E5 flybys. The ground tracks of the spacecraft trajectories are close to being perpendicular to the direction of the fissures and located close to the known gas vent (Figure 2). This allows the model to reproduce the observations even without accounting for the gas production by the Tiger Stripes.

The modeled total source rates as well as the contribution of the Tiger Stripes to the plume's production rate are presented in Tables 4 and 5. Below is the comparison of the model results with the INMS and UVIS measurements.

4.1. INMS

In this work we have applied the multiplume model to analyze INMS E3 (closest approach on 12 March 2008, 19:06:12 UTC) and E5 (closest approach on 9 October 2008, 19:06:43 UTC) observations [*Teolis et al.*, 2010]. Comparisons of the model fits with the observations are presented in Figure 3. The fits are consistent with the observations for both Cases 1 and 2. As shown in Figure 2, the direction of the flyby ground tracks are almost perpendicular to that of the fissures, which makes it very difficult to distinguish the contribution of the vent sources from that of the Tiger Stripes to Enceladus' exosphere.

The amount of the observational data is not sufficient to constrain production rates of all sources. For example, the vent VII is located extremely far from the ground tracks of the flybys (Figure 2), which makes its contribution to the INMS measurements insignificant. As a result, it is impossible to derive the source rate of this vent using the available data. For this reason, our estimations (Tables 4 and 5) represent the lower limits of the fissure and jet source rates for these data sets.

4.2. UVIS

We have applied the multiplume model to analyse UVIS 2005, 2007, and 2010 observations (Table 6). Comparisons of the model results with the observations are presented in Figures 4–7.

The model is consistent with UVIS 2005 measurements for both Cases 1 and 2 as shown in Figure 4. As in the case of INMS E3 and E5 discussed above, this can be explained by the orientation of instrument's line-of-sight direction that is almost perpendicular to that of the Tiger Stripes that is indicated in Figure 2.

Analysis of UVIS 2007 and 2010 observations suggests an important role of the Tiger Stripes in formation of Enceladus' exosphere, as described below in more detail.

Table 4. Modeled Total Production Rate and Primary Sources Obtained Without Accounting for the Gas Production by Tiger Stripes

Observation	Primary Vent	Total Production Rate (s^{-1})
INMS E3	II, VI	1.3×10^{28}
INMS E5	II, VI	2.9×10^{28}
UVIS 2005	I, II, III, IV, VI	1.1×10^{28}
UVIS 2007	I, II, III, IV, VI	9.7×10^{27}
UVIS 2010	I, II, III, IV, VII	3.9×10^{28}

4.2.1. UVIS 2007

The comparison of the model fits with the UVIS measurement is presented in Figure 5. Our calculations suggest that the total ejection rates into Enceladus's plume are 9.7×10^{27} s^{-1} and 6.7×10^{27} s^{-1} for Cases 1 and 2, respectively.

The modeled opacity calculated for Case 1 has a dip at elapsed time (the time starting the observation) of 448.9 s

Table 5. Modeled Total Production Rate and Primary Sources Obtained With the Gas Production by Tiger Stripes

Observation	Primary Vent	Total Production Rate (s^{-1})	Contribution of the Tiger Stripes
INMS E3	II, VI, Damascus (extra)	6.4×10^{27}	23%
INMS E5	II, VI, Damascus (extra)	1.4×10^{28}	32%
UVIS 2005	III, IV, Damascus (extra)	8.3×10^{27}	24%
UVIS 2007	I, II, III, V, VII, Bagdad (extra), Cairo (extra), Damascus (extra)	6.7×10^{27}	24%
UVIS 2010	I, III, IV, VI, VII, Alexandria, Cairo, Cairo (extra), Bagdad (extra)	2.9×10^{28}	25%

that is absent in Case 2. This suggests that UVIS observations at this elapsed time are dominated by the gas produced in the Tiger Stripes. According to our model, the measurement is dominated by gas ejected from a combination of Bagdad (extra), Cairo (extra), and Damascus (extra) fissures.

As shown in Figure 5, the peaks in the UVIS data measured at elapsed times of 449.8 and 450.8 s cannot be reproduced with our model. During this time interval, the UVIS instrument's line of sight scans the exosphere above vents II and III, which produce a peak in our model solution. So the observed peaks could be explained by either or both small variations of the vent locations and/or directions from assumed ones or by contribution of the unknown gas sources. To test this hypothesis, we have shifted locations of the vents II and III (Table 7), which allowed the model to reproduce the peaks with the total source rate of 7.4×10^{27} s^{-1} and contribution of the distributed sources along the Tiger Stripes of 28%. There is not enough statistical information for us to constrain the locations and directions of the sources. The presented example is an illustration of the effect that the source location has on the exospheric population.

The change of the slope in the UVIS measurement at elapsed time of 452 s as well as the general undershooting of the model results at elapsed times above ~451 s cannot be explained by any of the known vents, fissures, or background gas distribution. Our modeling suggests existence of an additional gas source located somewhere along the line of sight. In more detail the location of the possible source is discussed in section 4.2.2 and is presented in Figure 6.

4.2.2. UVIS 2010

Comparison of the model results with the observation is presented in Figure 6. The modeled column density and the observed occulted signal [*Hansen et al.*, 2011] have been related using the water absorption coefficient by *Mota et al.* [2005]. The model simulations suggest the total gas production rates of 3.9×10^{28} s^{-1} and 2.9×10^{28} s^{-1} for Cases 1 and 2, respectively.

The modeled occultation signal calculated for Case 1 has a dip at the elapsed time of 568.9 s when UVIS scans Enceladus' exosphere between vents IV and VIII. The dip is absent in Case 2. The ground track of the corresponding UVIS line of sight intersects Alexandria, which suggests that gas production from this fissure dominates UVIS measurements at this elapsed time.

As in the case of UVIS 2007, the modeled occultation signal is below the measured one at large elapsed times. The peak as well as the change of the slope of the measured occultation signal at the elapsed time

Table 6. Type and Start Times of the Analyzed UVIS Observations

Observation Time (UTC)	Type of Observation	References
14 July 2005, 19:55:22	Occultation of the star γ Orionis (Bellatrix)	*Hansen et al.* [2006], *Tian et al.* [2007]
24 October 2007, 16:59:50.3	Occultation of the star ζ Orionis (Alnitak)	*Hansen et al.* [2008]
18 May 2010, 5:51:44.45	Occultation of the Sun. The measurement has been performed using the solar occultation port of the extreme ultraviolet channel.	*Hansen et al.* [2011]

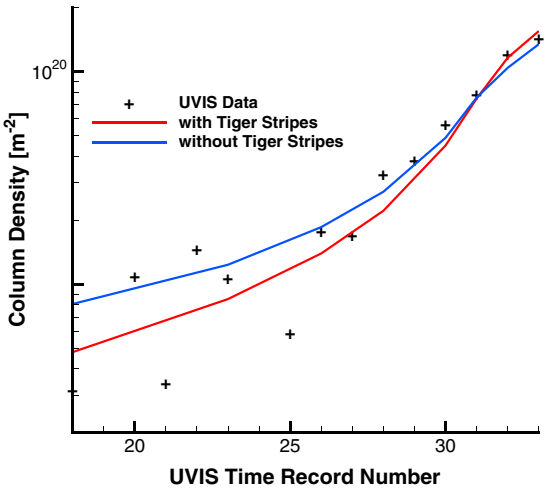

Figure 4. Comparison of the model results with UVIS 2005 [*Hansen et al.*, 2006]. Even without accounting for the gas production due to Tiger Stripes, the modeled column density is consistent with UVIS measurement.

of ~620 s suggests existence of an additional source. The source should be located at the region where its contribution is measured by UVIS at elapsed times more than 452 s and 619 s during UVIS 2007 and 2010 observations, respectively. A rough location of the new suggested source is presented in Figure 6.

The suggested source is located within a fracture, which suggests a geological activity of the area. We have tested the hypothesis of existence of the source by including it into our model. The comparison of the model results with UVIS 2007 and 2010 observations are presented in Figure 7. Accounting for the suggested source allowed the model to reproduce the measurements at large elapsed times with the total sources rates of 9.3×10^{27} s^{-1} and 2.5×10^{28} s^{-1} for UVIS 2007 and 2010, respectively.

5. Conclusion

In this work we investigate the effect of various sources in the Tiger Stripe region on water vapor distribution in Enceladus' exosphere. For this purpose, we have updated our multiplume model [*Tenishev et al.*, 2010] by including gas production from elongated fissures that simulate sources along all four Tiger Stripes.

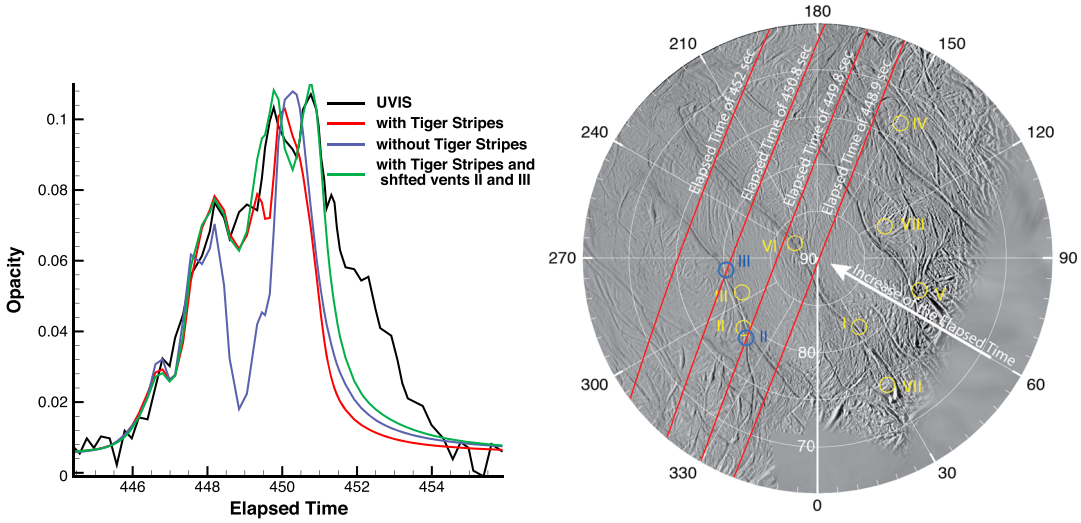

Figure 5. (left) Comparison of the model results with UVIS 2007 observation [*Hansen et al.*, 2008]. Without accounting for the gas production from the Tiger Stripes, the model does not reproduce the UVIS scan at the elapsed time of 448.9 s, when UVIS scans Enceladus' exosphere between vents IV and VI and above all four fissures. The model fit does not reproduce peaks in the UVIS data at the elapsed times of 449.8 and 450.8 s with the surface distribution of the known vents. Instead, the modeled opacity has a maximum between those elapsed times that is due to vents II and III. By shifting the locations of the vents II and III, the model was able to recover the peaks in the UVIS data. There is not enough statistical information that would allow us to constrain the locations of the vents, and the presented example is just an outline of the effect that variation of the source locations can have on the distribution of the volatiles in the exosphere. The change of the slope in UVIS data at the elapsed time of ~452 s as well as the general undershooting of the model results for the elapsed times above 451 s suggests existence of an additional source. (right) The plot presents the ground tracks of the UVIS 2007 line of sights and locations of the known vents (yellow circles) [*Spitale and Porco*, 2007] as well as the example of the alternative locations of the vents II and III (blue circles).

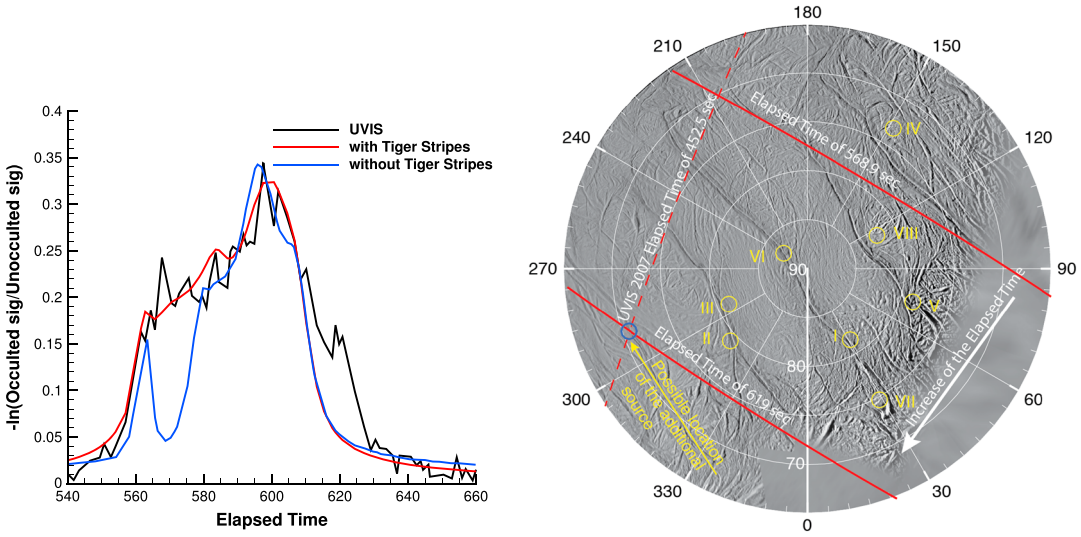

Figure 6. (left) Comparison of the model results with the UVIS 2010 observations [*Hansen et al.*, 2011]. Without accounting for the gas production from the Tiger Stripes, the modeled occulted signal has a dip at the elapsed time of 568.9 s. This elapsed time corresponds to the UVIS scan of the exosphere between vents IV and VIII. A model fit that is consistent with the observation can be obtained by accounting for the gas production from Alexandria. The peak in the observed occulted signal at the elapsed time of ~620 s suggests the existence of an additional source. (right) The plot presents the ground tracks of the UVIS 2010 line of sight as well as the locations of the known plume sources [*Spitale and Porco*, 2007]. The suggested previously unidentified source should be located in the region where its contribution is measured by UVIS at elapsed times more than 452 s and 619 s during UVIS 2007 and 2010 observations, respectively. The plot presents a rough location of the suggested source. The images made by Cassini indicate that the source is located within a fissure that suggests a geological activity of the area.

The model results presented in the paper clearly demonstrate the importance of the water vapor sources along the Tiger Stripes contributing to the gas distribution in the exosphere. By adding these sources, we have achieved a better agreement of the model results with the observations than in our previous work by *Tenishev et al.* [2010]. Without accounting for the gas production from the fissures, it is impossible to reproduce UVIS 2007 and 2010 observations.

The orientation of the spacecraft trajectory during INMS E3 and E5 and the line of sight during UVIS 2005 measurements allows one to reproduce the observations without including the effect of the Tiger Stripes. But accounting for the gas production from the fissures (Case 2) results in a decrease of the total gas

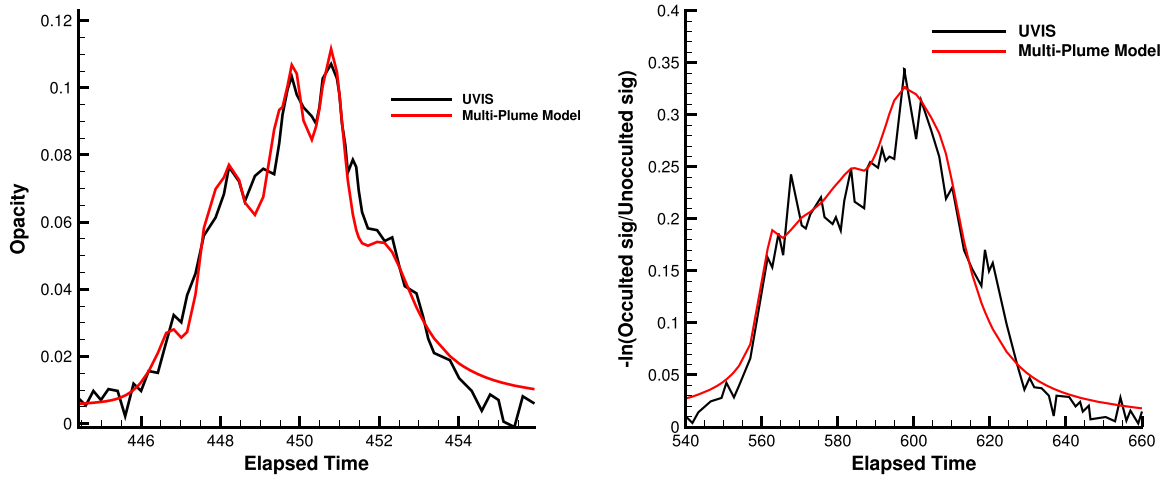

Figure 7. Comparison of the model results with UVIS (left) 2007 and (right) 2010 observations. For this comparison, we have included the effect of the extra source suggested in Figure 6 into the simulation. Accounting for the source allowed the model to reproduce the observations in the whole range of the elapsed times. The locations of the individual vents are as in *Spitale and Porco* [2007] except those for vents II and III, which are from Table 7.

Table 7. Locations of the Vents II and III That Reproduce the UVIS 2007 Observations

		Position on the surface	
Vent	Tiger Stripe	Lat.[a]	W. Lon.[a]
II	Damascus	78.6	318.3
III	Damascus	80.2	277.4

[a]Latitudes (Lat.) are planetographic and longitudes (W. Lon.) increase toward the west.

production by 25–50% over Case 1, where the effect of the fissures has been neglected. The Tiger Stripes' contribution varied in the range of 23–32% as shown in Tables 4 and 5.

The results of our simulations suggest the existence of the previously unidentified source that is needed to reproduce the UVIS 2007 and 2010 observations at large elapsed times. The possible location of the source is presented in Figure 6. Obtained by accounting for the suggested source, the model results are in agreement with the UVIS 2007 and 2010 observations for the whole interval of the elapsed times as shown in Figure 7.

The analysis performed includes observations made between 2005 and 2010. The calculated total gas production rate varies in the range of (9.7–39) $\times 10^{27}$ s^{-1} and (6.4–29) $\times 10^{27}$ s^{-1} for Cases 1 and 2, respectively. Even though the calculated source rates are only lower limit estimates, the variation suggests a time dependency of Enceladus' plume source rate [*Tian et al.*, 2007; *Waite et al.*, 2006; *Spencer*, 2013; *Hedman et al.*, 2013; *Hurford et al.*, 2009, 2012; *Smith et al.*, 2010; *Saur et al.*, 2008].

Acknowledgments
The authors would like to thank Candy Hansen for her valuable help in preparing the paper. Support for this work was provided by grant NNX08AP94G from the NASA Cassini Data Analysis Program. The data presented in the paper can be requested from Valeriy Tenishev (vtenishe@umich.edu).

References

Burger, M. H., E. C. Sittler, R. E. Johnson, H. T. Smith, O. J. Tucker, and V. I. Shematovich (2007), Understanding the escape of water from Enceladus, *J. Geophys. Res.*, *112*, A06219, doi:10.1029/2006JA012086.

Dong, Y., T. W. Hill, B. D. Teolis, B. A. Magee, and J. H. Waite (2011), The water vapor plumes of Enceladus, *J. Geophys. Res.*, *116*, A10204, doi:10.1029/2011JA016693.

Goguen, J. D., et al. (2013), The temperature and width of an active fissure on Enceladus measured with Cassini VIMS during the 14 April 2012 south pole flyover, *Icarus*, *226*(1), 1128–1137.

Hansen, C. J., L. Esposito, A. I. F. Stewart, J. Colwell, A. Hendrix, W. Pryor, D. Shemansky, and R. West (2006), Enceladus' water vapor plume, *Science*, *311*(5766), 1422–1425.

Hansen, C. J., L. W. Esposito, A. I. F. Stewart, B. Meinke, B. Wallis, J. E. Colwell, A. R. Hendrix, K. Larsen, W. Pryor, and F. Tian (2008), Water vapour jets inside the plume of gas leaving Enceladus, *Nature*, *456*(7221), 477–479.

Hansen, C. J., et al. (2011), The composition and structure of the Enceladus plume, *Geophys. Res. Lett.*, *38*, L11202, doi:10.1029/2011GL047415.

Hedman, M. M., P. D. Nicholson, M. R. Showalter, R. H. Brown, B. J. Buratti, and R. N. Clark (2009), Spectral observations of the Enceladus plume with CASSINI-VIMS, *Astron. J.*, *693*, 1749–1762.

Hedman, M. M., C. M. Gosmeyer, P. D. Nicholson, C. Sotin, R. H. Brown, R. N. Clark, K. H. Baines, B. J. Buratti, and M. R. Showalter (2013), An observed correlation between plume activity and tidal stresses on Enceladus, *Nature*, *500*(7461), 182–184.

Howett, C. J. A., J. R. Spencer, J. Pearl, and M. Segura (2011), High heat flow from Enceladus' south polar region measured using 10–600 cm^{-1} Cassini/CIRS data, *J. Geophys. Res.*, *116*, E03003, doi:10.1029/2010JE003718.

Hurford, T. A., B. G. Bills, P. Helfenstein, R. Greenberg, G. V. Hoppa, and D. P. Hamilton (2009), Geological implications of a physical libration on Enceladus, *Icarus*, *203*(2), 541–552.

Hurford, T. A., P. Helfenstein, and J. N. Spitale (2012), Tidal control of jet eruptions on Enceladus as observed by Cassini ISS between 2005 and 2007, *Icarus*, *220*(2), 896–903.

Ingersoll, A. P., and S. P. Ewald (2011), Total particulate mass in Enceladus plumes and mass of Saturn's E-ring inferred from Cassini ISS images, *Icarus*, *216*(2), 492–506.

Johnson, R. E., H. T. Smith, O. J. Tucker, M. Liu, M. H. Burger, E. C. Sittler, and R. L. Tokar (2006), The Enceladus and OH Tori at Saturn, *Astrophys. J.*, *644*(2), L137–L139.

Mota, R., et al. (2005), Water VUV electronic state spectroscopy by synchrotron radiation, *Chem. Phys. Lett.*, *416*(1–3), 152–159.

Postberg, F., J. Schmidt, J. Hillier, S. Kempf, and R. Srama (2011), A salt-water reservoir as the source of a compositionally stratified plume on Enceladus, *Nature*, *474*, 620–622.

Saur, J., N. Schilling, F. M. Neubauer, D. F. Strobel, S. Simon, M. K. Dougherty, C. T. Russell, and R. T. Pappalardo (2008), Evidence for temporal variability of Enceladus' gas jets: Modeling of Cassini observations, *Geophys. Res. Lett.*, *35*, L20105, doi:10.1029/2008GL035811.

Smith, H. T., R. E. Johnson, M. E. Perry, D. G. Mitchell, R. L. McNutt, and D. T. Young (2010), Enceladus plume variability and the neutral gas densities in Saturn's magnetosphere, *J. Geophys. Res.*, *15*, A10252, doi:10.1029/2009JA015184.

Spencer, J. (2013), Solar system: Saturn's tides control Enceladus' plume, *Nature*, *500*(7461), 155–156.

Spencer, J. R., and F. Nimmo (2013), Enceladus: An active ice world in the Saturn system, *Annu. Rev. Earth Planet. Sci.*, *41*, 693–717.

Spencer, J. R., A. C. Barr, L. W. Esposito, P. Helfenstein, A. P. Ingersoll, R. Jaumann, C. P. McKay, F. Nimmo, and J. H. Waite (2009), *Saturn From Cassini-Huygen*, Chap. Enceladus: An Active Cryovolcanic Satellite, 683 pp., Springer, Berlin.

Spencer, J. R., C. J. A. Howett, A. Verbiscer, T. A. Hurford, M. Segura, and D. C. Spencer (2013), Enceladus heat flow from high spatial resolution thermal emission observations, EPSC Abstracts EPSC2013-840-1 paper presented at Eur. Planet. Sci. Congr. 2013, vol. 8.

Spitale, J. N., and C. C. Porco (2007), Association of the jets of Enceladus with the warmest regions on its south-polar fractures, *Nature*, *449*, 695–697.

Tenishev, V., M. R. Combi, B. D. Teolis, and J. H. Waite (2010), An approach to numerical simulation of the gas distribution in the atmosphere of Enceladus, *J. Geophys. Res.*, *115*, A09302, doi:10.1029/2009JA015223.

Teolis, B., M. E. Perry, B. Magee, J. Westlake, and J. H. Waite Jr. (2010), Detection and measurement of ice grains and gas distribution in the Enceladus plume by Cassini's ion neutral mass spectrometer, *J. Geophys. Res.*, *115*, A09222, doi:10.1029/2009JA015192.

Tian, F., A. I. F. Stewart, O. B. Toon, K. W. Larsen, and L. W. Esposito (2007), Monte Carlo simulations of the water vapor plumes on Enceladus, *Icarus*, *188*(1), 154–161.

Waite, J. H., et al. (2006), Cassini ion and neutral mass spectrometer: Enceladus plume composition and structure, *Science*, *311*(5766), 1419–1422.